How dynamical clustering triggers Maxwell's demon in microgravity

E. Opsomer, M. Noirhomme, N. Vandewalle, and F. Ludewig
GRASP, Physics Department B5a, University of Liège, B-4000-Liège, Belgium
(Received 26 November 2012; revised manuscript received 6 May 2013; published 10 July 2013)

In microgravity, the gathering of granular material can be achieved by a dynamical clustering whose existence depends on the geometry of the cell that contains the particles and the energy that is injected into the system. By compartmentalizing the cell in several subcells of smaller volume, local clustering is triggered and the so formed dense regions act as stable traps. In this paper, molecular dynamics simulations were performed in order to reproduce the phenomenon and to analyze the formation and the stability of such traps. Depending on the total number N of particles present in the whole system, several clustering modes are encountered and a corresponding bifurcation diagram is presented. Moreover, an iterative model based on the measured particle flux F as well as a theoretical model giving the asymptotical steady states are used to validate our results. The obtained results are promising and can provide ways to manipulate grains in microgravity.

DOI: 10.1103/PhysRevE.88.012202 PACS number(s): 45.70.Qj, 05.45.−a, 02.60.Cb, 05.70.Fh

I. INTRODUCTION

When granular material is vertically driven, the system rapidly reaches a steady-state for which the injected energy and the dissipated energy perfectly outbalance over one period of oscillation [1]. Each collision between particles causes an energy loss that can be quantified via the coefficient of restitution ε. Nevertheless, for strong external forcing, high isotropic velocities are observed and the media behaves like a macroscopic dissipative gas. When such a granular gas is generated in a cell that is compartmented by a vertical wall allowing exchange through a slit, a symmetry breaking can appear under certain conditions [2,3]. Indeed, the grains spontaneously start to gather in the same compartment, which can naïvely be related to a sudden drop of the system's entropy. By analogy, this phenomenon is referred to as the granular pendant of Maxwell's demon. Different cell geometries such as cylindric systems [4] and grids [5] can be used, but the relevant physical mechanism remains the same.

In microgravity, granular materials can be gathered by a clustering [6–8]. Clustering is the tendency of a granular material to form dense and slow regions that can trap new incoming grains. While dissipative nature of the collisions are the main motor of the phenomenon, one can make a differentiation between the *classical clustering*, referring to the cooling of granular media [9], and the *dynamical clustering*, which is a condensed steady-state in a driven granular system [10]. Indeed, the first one is obtained through a long process of successive collisions that dissipate the energy and slows down the grains so that nearly immobile stripe-like regions are formed. On the other hand, the second type relies on a permanent energy injection (at the walls) that counterbalances the dissipation. This assures the equilibrium between the dense cluster phase in the center of the system and the gas phase surrounding it. If the energy supply is stopped, the dynamical cluster evaporates and the particles spread in the entire system until a cooling begins. Figure 1 describes these different clustering dynamics via a Kolmogorov-Smirnov (KS) test that confronts the particle distribution with a uniform law. If the test's value is above the threshold, the hypothesis of uniformity is refuted and clustering is observed. Data is obtained by prolonging earlier simulations of granular gases [11] and stopping the driving in the system after 10 seconds. The gray (red) KS curve indicates that dynamical clustering is detected until $t = 10$ s, when the energy injection is stopped. As the cluster evaporates, the KS curve sharply drops under the threshold (black line), and the system evolves into a gas state that rapidly starts to cool down. The KS curve increases and crosses the threshold again at about $t = 15$ s, which corresponds to the very beginning of a classical clustering.

Dynamical clustering has been observed in horizontal 2D cells [12], parabolic flights, and rocket missions [10] that have been reproduced and completed numerically using molecular dynamics simulations [13]. Moreover, the European Space Agency (ESA) is doing intensive research on the behavior of granular media in microgravity. In particular, the SpaceGrains project [14] focuses on cluster formation and Maxwell's demon. In the main cell of the SpaceGrains device, N spherical particles with a radius R are enclosed in a box of dimensions $60 \times 30 \times 30$ mm^3. Two pistons are oscillating in phase opposition with an amplitude A and a frequency f around their respective positions z_1 and z_2. The distance L between z_1 and z_2 can be modified in order to tune the accessible volume of the system. Figure 2 provides a brief description of the systems parameters.

This work aims to investigate the formation of traps and the occurrence of Maxwell's demon in microgravity by numerical simulations. In order to provide predictive results, the simulated system is based on a compartmentation of the main cell of the ESA's SpaceGrains project. We discuss the triggering role of clustering for Maxwell's demon under microgravity conditions and present two theoretical models reproducing the observed phenomena.

II. NUMERICAL APPROACH

The realized simulations are based on a molecular dynamics (MD) approach. This model is widely used in soft-matter physics and especially in the simulation of granular materials [13,15] because of its capacity to handle efficiently multiple collisions that are unavoidable in dissipative systems. Normal forces F_{ij}^n are composed by a repulsive F_{ij}^{rep} and a dissipative F_{ij}^{dis} component. The repulsive component follows

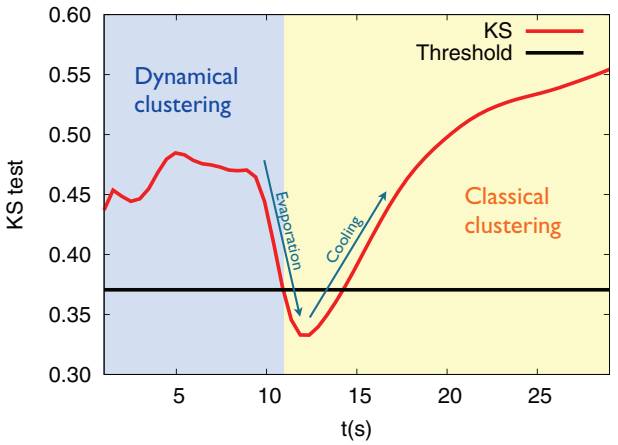

FIG. 1. (Color online) The KS test, represented by a gray (red) curve, indicates the evaporation of a dynamical cluster in microgravity once the driving is stopped (at $t = 10$ s). After a short period of gas phase, a cooling process is observed.

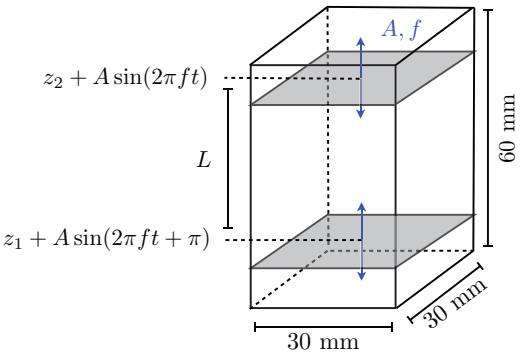

FIG. 2. (Color online) Sketch of ESA's SpaceGrains cell. Spherical particles of radius R are enclosed in a $60 \times 30 \times 30$-mm^3 box. Two pistons are oscillating in phase opposition with an amplitude A and a frequency f around their respective positions z_1 and z_2. The distance $L = |z_2 - z_1|$ can be modified in order to tune the accessible volume of the system.

Hooke's law,

$$F_{ij}^{\text{rep}} = -k_n \delta_{ij}, \tag{1}$$

where δ_{ij} is the surface-to-surface distance between two solids, i and j. The constant k_n is the numerical normal stiffness, which is determined by fixing the maximum particle deformation at $R/100$. The dissipative component is taken into account by viscous forces according to the following law:

$$F_{ij}^{\text{dis}} = -\gamma_n(k_n, \varepsilon)\frac{\partial \delta_{ij}}{\partial t}, \tag{2}$$

where the viscous constant γ_n is function of k_n and the restitution coefficient ε. This restitution coefficient is used for both grain-grain and grain-wall collisions. Tangent forces F_{ij}^t are bounded and depend on the relative tangent velocities v_{ij}^t between the colliding solids i and j. One has

$$F_{ij}^t = -k_t v_{ij}^t \quad \text{and} \quad \left\| F_{ij}^t \right\| \leqslant \mu F_{ij}^n, \tag{3}$$

where μ is a friction coefficient and k_t a purely numerical constant. A complete description of this MD approach is given by Taberlet [16].

III. NUMERICAL RESULTS

A. Observations

We realized a large number of numerical simulations reproducing a compartmentalized version of SpaceGrains. Our cell is filled homogeneously with N spherical particles of radius $R = 0.5$ mm. The average distance L between the pistons is fixed at 50 mm. In addition to the basic cell, two orthogonal walls of height $h = 30$ mm are inserted in the center of the cell, as displayed in Fig. 3. This way four subcells are formed. The system is periodically driven with an amplitude $A = 5$ mm and a frequency $f = 10$ Hz. The granular media is shaken up and grains are free to travel from one compartment to another. The observed dynamics depend strongly on N. Indeed, for a small number of grains, the whole system remains in a gas state. The particles travel with high speed and spread homogeneously. For a larger N, a cluster forms and the grains start to gather in the same compartment. This cluster keeps growing and traps the incoming grains until the compartment is filled. When more grains are injected in the system, a second cluster can form and a competition between two traps is observed. Moreover, the second cluster mostly forms in the diagonal neighboring compartment of the first cluster. A further increase of N leads then to the formation of three and, finally, four clusters. This last regime can also be considered as a second homogenous state since all particles are distributed equally in the system. Figure 3 gives a brief overview of the encountered dynamics for an increasing total number of particles. The top row presents the simulated systems while the bottom row shows the top views of the corresponding cells.

B. Filling measures

In addition to its dependency on the total number of grains, the formation of the traps in the system is a dynamical process that evolves continuously. Tracking the filling number n_1, n_2, n_3, and n_4 of the four compartments allows us to evaluate the stability of the observed clusters. This measure implies a temporal discretization that is achieved by using as unit time step the oscillation period T. Figure 4 presents in black lines the evolution of n_i as a function of the number of time steps t. The total number of grains in the system is fixed at $N = 4200$ (two traps are formed). Other colors correspond to complementary simulations explained in Secs. V and VI.

For most simulated systems, a steady-state is reached after 1200 periods. Thanks to the obtained final compartment fillings, a bifurcation diagram describing the different values of n_1, n_2, n_3, and n_4 as a function of N is established and presented in Fig. 5. Until a certain threshold N_c (left dashed line), no trap is observed and all compartment fillings are roughly equal. Then, abruptly, a very neat bifurcation corresponding to the cluster formation occurs. Almost all grains gather in a single compartment leaving three others poorly filled. Recent results [11] allow us to predict the apparition of such dynamical clustering. Indeed, for a given system of maximal volume $v = \ell^2(L + 2A)$, the clustering criterion is given by

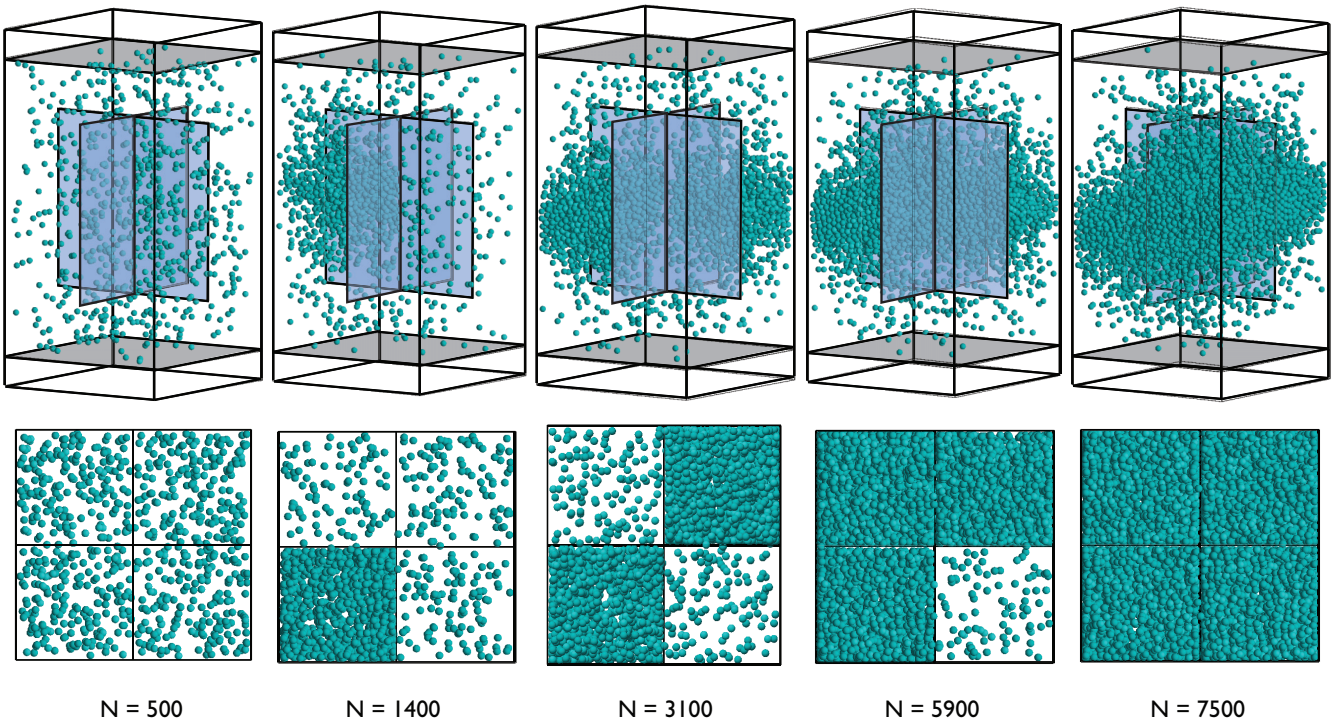

FIG. 3. (Color online) Dynamics of the compartmentalized system for increasing N. The top row displays snapshots of the simulated cells. For high enough filling numbers, clustering is encountered and grains gather in one (or more) compartment(s). The bottom row shows the top view of the corresponding cells.

the following condition:

$$\frac{\delta(L,\ell,A)}{R} > \frac{\xi(\varepsilon)}{3\phi}\left(\frac{1}{1-c\phi}\right), \tag{4}$$

where δ is the characteristic length scale of the cell, c is a constant, and the function ξ depends only on ε. The packing fraction ϕ is defined by

$$\phi = N\frac{4\pi R^3}{3v}. \tag{5}$$

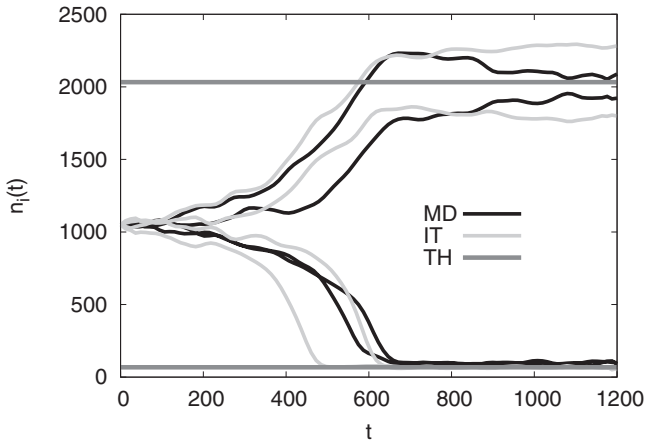

FIG. 4. Evolution of the filling number of the different compartments over 1200 periods in a system of 4200 grains. Molecular dynamics simulations are represented in black, the iterative model in light gray, and the asymptotic results are displayed as two dark-gray horizontal lines.

By introducing the geometrical parameters of a compartment into Eq. (4), the local threshold is found to correspond to a filling number $N_c = 808$, denoted by a vertical dashed line in Fig. 5. This single cluster regime persists until a filling number of approximatively 3000 particles, when it is replaced by a regime with two traps. This region is far more noisy, so that the relative compartment fillings n_i/N spread around the value of 0.5. Systems with three clusters are recorded for $N > 4200$;

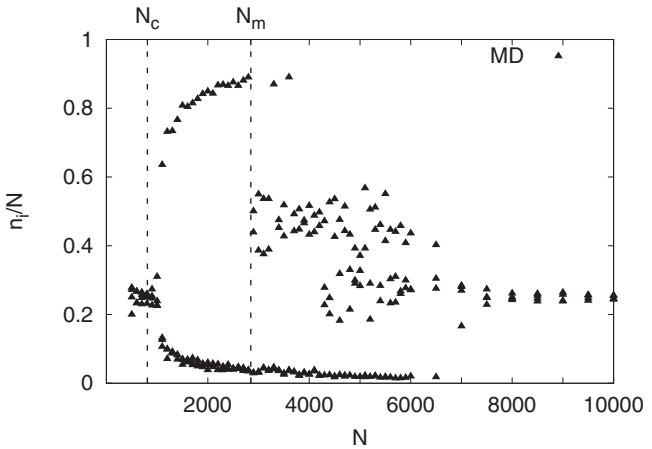

FIG. 5. Bifurcation diagram of the encountered final states of the system. After 1200 periods, the filling ration n_i/N is plotted with black triangles against the total number of particles N. The first bifurcation is predicted by Eq. (4) at a value of $N = 808$. The vertical dashed lines correspond to the critical values of N_c and N_m discussed in the main text.

however, they are rarely observed and seem less stable. Finally, above 6000 grains, the system becomes homogenous again, i.e., clustering takes place in all compartments.

C. Analogy with a granular fountain

These first results described in Sec. III present a lot of similarities with what is found for a granular fountain [17]. In a granular fountain, granular material is driven in a compartmented cell under gravity. Each compartment can communicate with its neighbors either through a slit at a certain height h or by the means of another slit at the bottom of the cell. Like our system, a granular fountain exhibits several trapping modes and multistable regimes. Moreover, the same discontinuous transition is observed on their respective bifurcation diagrams when the first trap occurs. Despite these intriguing analogies, several differences due to the experimental conditions are noted. Indeed, gravity has an impact on the symmetry of the system. The granular fountain as well as our system present two openings per compartment. However, the fluxes present in the fountain are influenced by gravity and have unequal intensities while they are perfectly symmetric in our cell. One can also note that fixed driving parameters were used in the microgravity simulations and that phase transitions are induced by the variation of the number of particles N. Since higher filling fractions can be obtained this way, additional features such as dynamical clustering, crystallization, and overflowing compartments can be generated.

IV. GRANULAR FLUXES

A. Mean flux function

The formation mechanisms of the traps and the complex dynamics of the system are linked to the number of grains that the different compartments exchange. In order to quantify this particle flux, each time a compartment filled with n grains is encountered, the number X_n of grains leaving it for a neighboring compartment is recorded. For a fixed n, the obtained distribution of outgoing grains follows roughly a binomial law

$$X_n \sim \mathcal{B}(n, p_n), \tag{6}$$

where p_n denotes the probability that a grain leaves a compartment filled with n particles. Indeed, this binomial behavior can be interpreted as following: At each time step, the binary-experience *leave* versus *stay* is repeated for each of the n grains. Since the event *leave* has a probability p_n, the random variable X_n follows a binomial distribution. Accordingly, the escape probability is given by the following relation:

$$p_n = \frac{\langle X_n \rangle}{n}, \tag{7}$$

where the mean flux $\langle X_n \rangle$ is the average value of X_n. Figure 6 represents with black dots the evolution of $\langle X_n \rangle$ for an increasing number of grains. For low n, the agitation is strong in the cell and the flux raises up to a maximum value. After that peak, a cluster tends to form; accordingly, the flux drops and becomes nearly constant once the critical value N_c is reached. At that point, the trap becomes stable. The flux

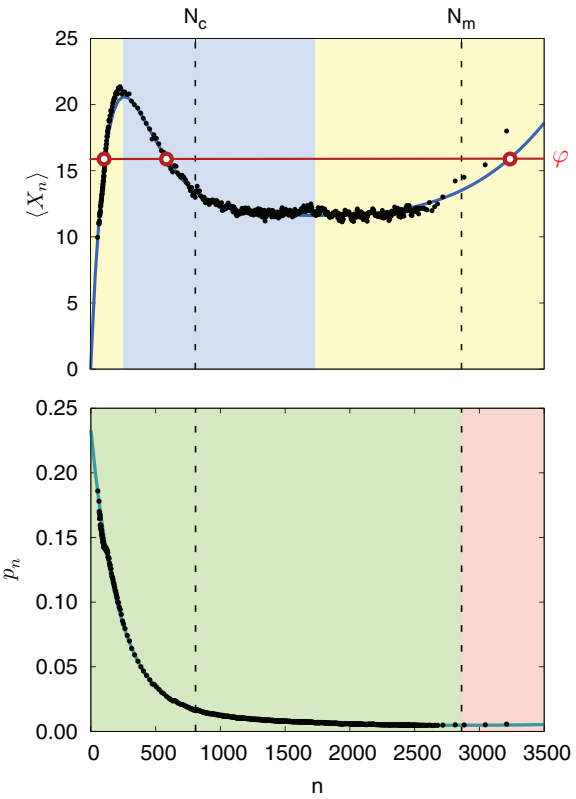

FIG. 6. (Color online) Top figure describes $\langle X_n \rangle$ in black dots and its fit, the mean flux function $F(n)$, in medium gray (blue) for an increasing number of grains. F can be subdivided into three invertible functions in each shaded zone. Moreover, a fixed flux φ can correspond to three fillings as presented by the light gray (red) horizontal line. Bottom figure shows the corresponding evolution of the measured escape probability in black dots and the fitted p_n with a solid gray (green) line.

remains low until the compartment is abundantly filled. The distance between cluster and borders of the compartment gets then smaller and grains can more easily escape. Moreover, the increase of the flux can also be linked to the natural evaporation that is part of the formation mechanism of dynamical clusters. Note that qualitatively similar fluxes are observed in analog systems such as ratchets [18] and granular fountains [17]. However, the observed plateau is a particular feature of our system. An analytical function approaching this mean flux can be found using statistical arguments. For a low n, the escape probability can be approached by the linear combination of two exponential laws of base $0 < p < 1$.

$$p_n = C_1 p^{\gamma_g n(\sigma/\ell^2)} + C_2 p^{\gamma_c n(\sigma/\ell^2)}, \tag{8}$$

where σ/ℓ^2 is the dimensionless cross section of a particle and the coefficients C_1 and C_2 are free fitting parameters. The constants $\gamma_c = 0.14$ and $\gamma_g = 0.86$ model the density increase in the central part of the system under the hypothesis of normal distribution along the oscillation axis.

However, each compartment has a critical capacity, noted N_m, above which the escape probability is expected to increase. This can be modeled by a symmetrization of p_n about N_m that

is noted p_n^*. The mean flux function F is finally defined by

$$F(n) = np_n^*. \tag{9}$$

Fitting F on the average $\langle X_n \rangle$ leads then to a critical filling $N_m = 2849$ that corresponds to a packing fraction of 19%. This critical value is represented by the right dashed line in Fig. 5 and corresponds to a threshold beyond which a second trap can form. The obtained function F is plotted in gray (blue) in the top of Fig. 6 and is in good agreement with the data. The bottom of Fig. 6 shows the corresponding evolution of the measured escape probability in black dots and p_n^* in gray (green).

B. Geometrical coefficients

The relative positions of the compartments also have an impact on the grain exchanges. In order to determine the direction of the outgoing flux, the flux coefficients c_{ij} have to be introduced. They measure the fraction of the flux going from the compartment i to j when $i \neq j$ and have the value $c_{ij} = \{-1\}$ for $i = j$. These coefficients are evaluated on each simulation and then summarized in the following flux matrix:

$$\mathbf{C} = \begin{bmatrix} -1 & 0.46 & 0.46 & 0.08 \\ 0.46 & -1 & 0.08 & 0.46 \\ 0.46 & 0.08 & -1 & 0.46 \\ 0.08 & 0.046 & 0.46 & -1 \end{bmatrix}. \tag{10}$$

The conservation of the total number of grains implies that summing on a row of **C** yields 0. Moreover, one can note that the exchange of particles is strong with direct neighbors and weak with the diagonal neighbors. This asymmetry explains why, in the case of a two-cluster system, both traps form in diagonal neighboring compartments. Indeed, this particular configuration minimizes the granular exchange between the clusters and allows, thus, an higher stability of the regime.

V. ITERATIVE MODEL

In order to realize efficiently a great number of simulations, a statistical model based on the mean particle flux has been elaborated. Using F and the flux coefficients c_{ij}, the evolution of the filling n_i of each of the i compartments can be determined according to the following equations:

$$\frac{\partial n_i}{\partial t} = \sum_{j=1}^{4} c_{ji} F(n_j), \tag{11}$$

with $1 \leqslant i \leqslant 4$ and t being the number of time steps. To take into account the statistical fluctuations and to avoid unstable stationary solutions, a stochastic noise term must be injected into Eq. (11). The fluctuations are represented through random variables ζ following a standard normal distribution. According to the Moivre-Laplace theorem, a global flux function can be described by

$$F_\zeta(n) = F(n) + \zeta \sqrt{F(n)(1 - F(n)/n)}. \tag{12}$$

The evolution of the number of grains in the different compartments is then given by Eq. (11), where $F(n_j)$ is replaced by $F_\zeta(n_j)$. For identical initial conditions, the results of this model are in good agreement with of our MD simulations. Indeed,

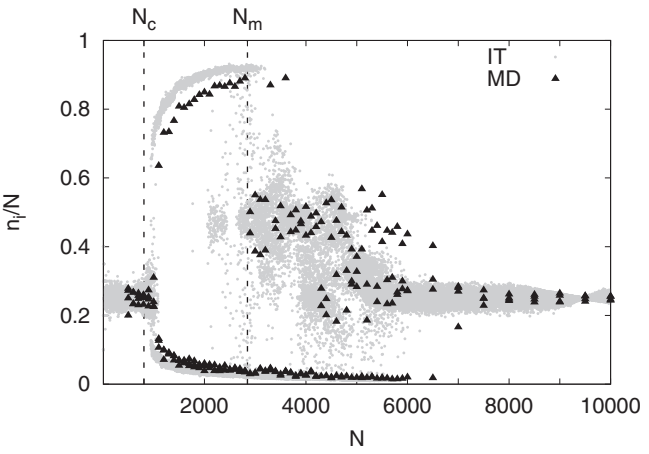

FIG. 7. Comparison between MD simulations described by black triangles and iterative model in light gray based on a limit normal assumption. Critical values N_c and N_m are represented by two dashed vertical lines.

Fig. 4 shows a similar evolution of the iterative approach in light gray and the MD data in black. Moreover, Fig. 7 displays the ratio n_i/N of grains present in each compartment i as a function of N after 1200 iterations. The molecular dynamics simulations are represented by black triangles while the iterative model is colored in light gray. Main branches of the bifurcation diagram are obtained.

VI. THEORETICAL MODEL

A. Stationary solutions

In analogy to earlier works [4,19,20], an asymptotic bifurcation diagram for a granular system in microgravity can be realized. Obviously, the final values of n_1,n_2,n_3, and n_4 are reached once the filling number of all compartments remains constant in time. By writing Eq. (11) in its matrix form, this condition becomes equivalent to

$$\mathbf{M}(\vec{F}) = \mathbf{C} \cdot \vec{F} = \vec{0}, \tag{13}$$

where $\vec{F} = [F(n_1), \ldots, F(n_4)]$. Since each row of the flux matrix sums up to zero, the kernel of $\boldsymbol{M}$ is the linear hull of the vector $\vec{1} = (1,1,1,1)$. Accordingly, stationary solutions are characterized by $\vec{F} = \varphi\vec{1}$, $\varphi \in \mathbb{R}$, and the fixed-point conditions become

$$\begin{cases} F(n_i) = \varphi \quad \forall i \in \{1, \cdots, 4\} \\ \sum_{i=1}^{4} n_i = N, \end{cases} \tag{14}$$

with φ being a constant particle flux. These conditions imply the conservation of the total number of particles coupled with an identical flux for all compartments.

B. Sum functions

Since the mean flux $F(n)$ presents both a minimum and a maximum, a same fixed value of φ can be obtain for up to three different fillings as presented in light gray (red) in Fig. 6. Indeed, $F(n)$ can only be inverted piecewise around the different extrema and for each section $l \in \{1,2,3\}$ the

respective inverse function is noted F_l^{-1}. In order to find the asymptotical compartment fillings for a fixed N, all possible combinations implying the three inverse functions and the four boxes have to be considered. For that purpose, the sum functions S_{ij} are introduced and defined by the following relations:

$$S_{ij}(\varphi) = i F_1^{-1}(\varphi) + j F_2^{-1}(\varphi) + k F_3^{-1}(\varphi), \qquad (15)$$

where $k = (4 - i - j)$ with $0 \leqslant i, j \leqslant 4$. The coefficients i, j, k give the effective of the corresponding filling number. Indeed, let φ_0 be a solution of $S_{ij}(\varphi) = N$. If one defines $z_l = F_l^{-1}(\varphi_0)$ for $l \in \{1,2,3\}$, the system is composed by i compartments of z_1 grains, j compartments of z_2 grains, and k compartments of z_3 grains.

C. Stability

The stability of the obtained solutions can be determined via the Jacobi matrix $\mathbf{J}$ relative to Eq. (11), which can be calculated from

$$\mathbf{J} = \mathbf{C} \cdot \mathbf{diag}\left[\left.\frac{\partial F}{\partial n}\right|_{n=n_1}, \ldots, \left.\frac{\partial F}{\partial n}\right|_{n=n_4} \right]. \qquad (16)$$

A solution $(n_1, \ldots, n_4)$ is stable if all the corresponding eigenvalues of the Jacobi matrix are negative or equivalently if

$$\max_{\lambda}\{\lambda | \det(\mathbf{J} - \mathbf{I}\lambda) = 0\} < 0. \qquad (17)$$

Figure 8 presents the stationary solutions of the system using the theoretical approach. Stable branches are described by thick dark gray and unstable by thin black lines. The MD simulations are represented by black triangles. Moreover, the stable solutions for a system of 4200 particles are also represented by two dark gray lines in Fig. 4.

Nevertheless, some differences are noted between the iterative and the theoretical model. This is due to the fact that the theoretical model represents the asymptotic steady state. By computing the iterative diagram for a large number of time steps (12 000) and all different initial conditions, both models converge as shown in Fig. 9.

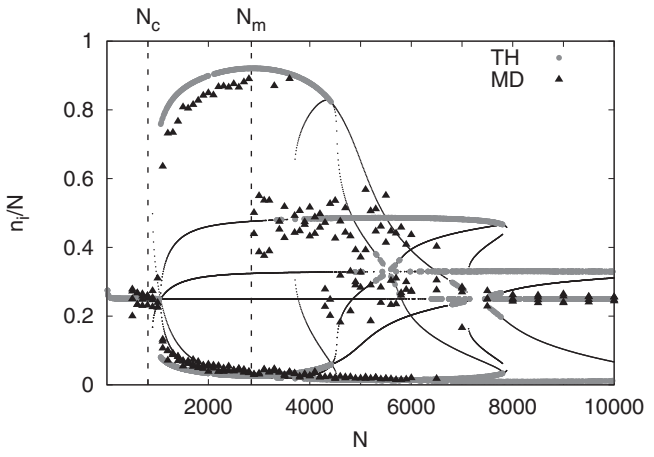

FIG. 8. Comparison between MD simulations (black triangles) and theoretical model. Stable branches are represented with thick dark gray and unstable with thin black curves.

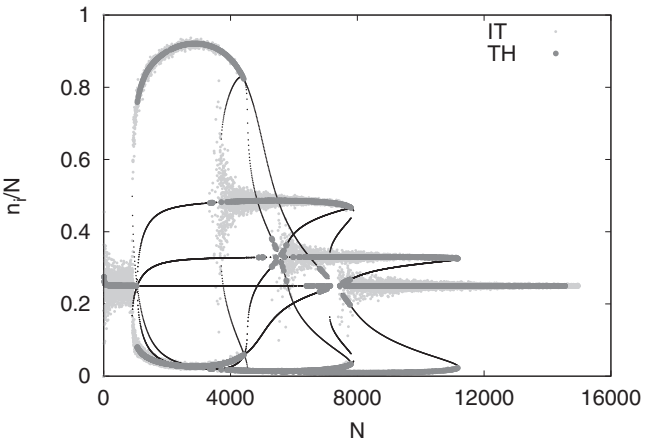

FIG. 9. Comparison between the iterative model in light gray and the theoretical model in dark gray. For a large enough number of iterations, both models converge to the same final states.

Moreover, in the multistable region ($N > 6500$), the measured data seemed to prefer the four-cluster state. This repartition is obviously triggered by the homogenous initial conditions that were used in the MD simulations. Indeed, the completed simulations presented in Fig. 9 recover the other branches.

VII. CONCLUSION AND PERSPECTIVES

In this paper, we proposed a particular cell geometry that allows us to produce Maxwell's demon in ESA's SpaceGrains project. Molecular dynamics simulations showed trapping in the different compartments that is triggered by dynamical clustering. Moreover, the presence of clustering and trapping could be predicted thanks to earlier theoretical results [11]. Many analogies with classical systems, such as granular fountains, granular clocks, and ratchets, have been observed and qualitatively similar flux functions were obtained. However, a nonnegligible, almost constant, residual flux was observed for intermediate filling fraction, so that usual models could not properly reproduce the dynamics. A bifurcation diagram recovering the totality of our simulations was presented.

An iterative stochastic model reproducing the systems evolution has been proposed and allowed a more efficient way to simulate the dynamics present in Maxwell's demon. Finally, we describe a theoretical model that gives the asymptotic stable states of the system. Mutlistable regions were expected, but given our initial conditions, a homogenous repartition of the particles is preferred. Note that for a high number of iterations the stochastic model converges to the asymptotic solutions.

Our results are promising because ratchets and others' transport mechanisms, providing ways to manipulate grains in microgravity, can be envisaged in the SpaceGrains experiment.

In the future, larger lattices of 9 or 16 compartments on could be realized. The major difference would be the presence of different fluxes depending on the compartment of interest. Indeed, the central compartments lose grains more easily than the ones in the corners. This could be modeled by either several

flux functions or by an adapted flux matrix. Other types of compartment arrangements (linear or cylindric) could easily be implemented and compared to our results. Moreover, the effect of the shape of the compartment itself on the flux dynamics could be studied. By using more complex aspherical particles, the influence of the interlocking [21] on Maxwell's demon could be investigated.

ACKNOWLEDGMENTS

This work has been supported by Prodex (Belspo, Brussels) and the European Space Agency program TT VIP-GRAN/SpaceGrains. We also thank the T-REX Morecar project (Feder, Wallonia) for supporting the development of our numerical model.

[1] S. Aumaítre, J. Farago, S. Fauve, and S. Mc Namara, Eur. Phys. J. B. **42**, 255 (2004).
[2] J. Eggers, Phys. Rev. Lett. **83**, 5322 (1999).
[3] A. Barrat and E. Trizac, Molecular Physics **101**, 11 (2003).
[4] K. van der Weele, Contemp. Phys. **49**, 157 (2008).
[5] S. Dorbolo *et al.*, Eur. J. Phys. **32**, 1465 (2011).
[6] Y. Li, M. Hou, and P. Evesque, J. Phys. Conf. Ser. **327**, 012034 (2011).
[7] N. Isert, C. C. Maaß, and C. M. Aegerter, Eur. Phys. J. E **28**, 205 (2009).
[8] J. J. Brey, F. Moreno, R. García-Rojo, and M. J. Ruiz-Montero, Phys. Rev. E **65**, 011305 (2001).
[9] I. Goldhirsch and G. Zanetti, Phys. Rev. Lett. **70**, 1619 (1993).
[10] E. Falcon, R. Wunenburger, P. Evesque, S. Fauve, C. Chabot, Y. Garrabos, and D. Beysens, Phys. Rev. Lett. **83**, 440 (1999).
[11] E. Opsomer, F. Ludewig, and N. Vandewalle, Europhys. Lett. **99**, 40001 (2012).
[12] A. Kudrolli, M. Wolpert, and J. P. Gollub, Phys. Rev. Lett. **78**, 1383 (1997).
[13] E. Opsomer, F. Ludewig, and N. Vandewalle, Phys. Rev. E **84**, 051306 (2011).
[14] ESA SpaceGrains project: http://www.spacegrains.org/
[15] S. Miller and S. Luding, Phys. Rev. E **69**, 031305 (2004).
[16] N. Taberlet, Ph.D. thesis, Université de Rennes I, 2005.
[17] D. van der Meer, K. van der Weele, and P. Reimann, Phys. Rev. E **73**, 061304 (2006).
[18] D. van der Meer, P. Reimann, K. van der Weele, and D. Lohse, Phys. Rev. Lett. **92**, 184301 (2004).
[19] D. van der Meer, K. van der Weele, and D. Lohse, Phys. Rev. E **63**, 061304 (2001).
[20] D. van der Meer, K. van der Weele, P. Reimann, and D. Lohse, J. Stat. Mech. (2007) P07021.
[21] F. Ludewig and N. Vandewalle, Phys. Rev. E **85**, 051307 (2012).